

University of Texas Rio Grande Valley

ScholarWorks @ UTRGV

---

Mathematical and Statistical Sciences Faculty  
Publications and Presentations

College of Sciences

---

3-4-2022

## Multiple Periodic Vibrations of Auxetic Honeycomb Sandwich Plate with 1:2 Internal Resonance

Shaotao Zhu

Jing Li

Zhijun Qiao

*The University of Texas Rio Grande Valley*, zhijun.qiao@utrgv.edu

Ji Zhou

Follow this and additional works at: [https://scholarworks.utrgv.edu/mss\\_fac](https://scholarworks.utrgv.edu/mss_fac)



Part of the [Mathematics Commons](#)

---

### Recommended Citation

Zhu, S., Li, J., Qiao, Z. et al. Multiple Periodic Vibrations of Auxetic Honeycomb Sandwich Plate with 1:2 Internal Resonance. *J Nonlinear Math Phys* (2022). <https://doi.org/10.1007/s44198-022-00043-y>

This Article is brought to you for free and open access by the College of Sciences at ScholarWorks @ UTRGV. It has been accepted for inclusion in Mathematical and Statistical Sciences Faculty Publications and Presentations by an authorized administrator of ScholarWorks @ UTRGV. For more information, please contact [justin.white@utrgv.edu](mailto:justin.white@utrgv.edu), [william.flores01@utrgv.edu](mailto:william.flores01@utrgv.edu).



# Multiple Periodic Vibrations of Auxetic Honeycomb Sandwich Plate with 1:2 Internal Resonance

Shaotao Zhu<sup>1,2</sup> · Jing Li<sup>1</sup> · Zhijun Qiao<sup>1,3</sup> · Ji Zhou<sup>4</sup>

Received: 3 December 2021 / Accepted: 12 February 2022  
© The Author(s) 2022

## Abstract

In this paper, we focus on the multiple periodic vibration behaviors of an auxetic honeycomb sandwich plate subjected to in-plane and transverse excitations. Nonlinear equation of motion for the plate is derived based on the third-order shear deformation theory and von Kármán type nonlinear geometric assumptions. The Melnikov method is extended to detect the bifurcation and multiple periodic vibrations of the plate under 1:2 internal resonance. The effects of transverse excitation on nonlinear vibration behaviors are discussed in detail. Evolution laws and waveforms of multiple periodic vibrations are obtained to analyze the energy transfer process between the first two order modes. Even quite small transverse excitation can cause periodic vibration in the system, and there can be at most three periodic orbits in certain bifurcation regions. The periodic orbits are classified into two families by tracing their sources. The study provides the possibility for the classification study on generation mechanism of system complexity and energy transfers between different modes.

**Keywords** Auxetic honeycomb sandwich plate · Multiple periodic vibrations · Bifurcation · Energy transfer · Internal resonance

## List of Abbreviations

NPR Negative Poisson's ratio  
TSDT Third-order shear deformation theory  
FSDT First-order shear deformation theory

---

✉ Jing Li  
leejing@bjut.edu.cn

<sup>1</sup> Interdisciplinary Research Institute, Faculty of Science, Beijing University of Technology, Beijing 100124, China

<sup>2</sup> Faculty of Information Technology, Beijing University of Technology, Beijing 100124, China

<sup>3</sup> School of Mathematical and Statistical Sciences, University of Texas Rio Grande Valle, Edinburg TX 78539, USA

<sup>4</sup> State Key Laboratory of New Ceramics and Fine Processing, School of Materials Science and Engineering, Tsinghua University, Beijing 100084, China

## 1 Introduction

Honeycomb sandwich structure is widely used in virtually every branch of modern industry due to its superior properties of light weight, high specific stiffness, high specific strength, good fatigue resistance and energy absorption [1]. A typical honeycomb sandwich structure consists of two (top and bottom) thin face sheets and a (middle) light-weight core layer, and usually the core is a polygonal lattice made of metal, paper or other materials. Honeycomb sandwich structure can be artificially designed to exhibit a unique range of physical and mechanical properties by selecting various materials or structures of core.

Auxetic materials, named by Evans [2], refer to materials with negative Poisson's ratio (NPR). As one of novel excellent promising metamaterials, auxetic materials have gradually captured the attention of numerous material engineers and scientists. An amount of work had done to achieve NPR, see [3–7] and references therein. A review on what Poisson's ratio means in the contemporary understanding of the mechanical characteristics of modern materials was assessed by Greaves et al. [8]. Lim [9] investigated the suitability of auxetic materials for load-bearing circular plates and showed that the optimal Poisson's ratio for minimizing the bending stresses was strongly dependent on the final deformed shape, load distribution, and the type of edge supports. Thereafter, three models for the shear correction factor of plates as a function of Poisson's ratio were proposed: an analytical model, a cubic fit model and a modified model [10], and the effect of auxeticity on shear deformation in thick plates was concerned. The effects of cell-wall thickness on the deformation mode of metallic auxetic reentrant honeycomb, and the effects of NPR on the crushing stress were clarified by Dong et al. [11].

In recent decades, the auxetic materials are increasingly used as the core in structural designs of honeycomb sandwich plates because of their engineering advantages over traditional materials, including increased indentation resistance [12, 13], plane strain fracture toughness [14, 15], crashworthiness [16] and high energy absorption [17–19]. Yang et al. [20] presented a comparative study of ballistic resistance of sandwich panels with aluminum foam and auxetic honeycomb cores. They found that the sandwich panel with auxetic core is far superior to the panel with aluminum foam core in ballistic resistance because of the material concentration at the impacted area due to the NPR effect. Imbalzano et al. [21] analyzed the equivalent sandwich panels composed of auxetic and conventional honeycomb cores with metal facets, and compared their resistance performances against impulsive loadings. Zhang et al. [22] studied nonlinear transient responses of an auxetic honeycomb sandwich plate under impact dynamic loads, and found that the honeycomb sandwich plate with NPR would be a better choice compared with the positive one.

As common structural elements, sandwich plates with auxetic honeycombs are widely used in aerospace, defense and other industries. The mechanical and dynamical properties of the plates have attracted attention of many researchers. For instance, Streck et al. [23] studied the dynamic response of a sandwich panel made of two face sheets and auxetic core, and considered the influence of filler

material on the effective properties of the sandwich panel. Zhu et al. [24] investigated the frequencies and energies of free vibrations and vibrations with the damping and in-plane force of a honeycomb sandwich plate with NPR. Quyen et al. [25] investigated the nonlinear free and forced vibration of auxetic sandwich cylindrical plate on visco-Pasternak foundations in thermal environment subjected to blast load. And the effects of geometrical parameters, visco foundations, initial imperfection, temperature increment, nanotube volume fraction and blast load on the nonlinear vibration characteristics of the plate were numerical studied.

Considerable progress has been made in the study of theory and application of nonlinear dynamic response and vibrations for various plates [22–26]. In the future studies, more attentions should be drawn on the multiple periodic vibrations of sandwich plates with auxetic honeycombs, and the following aspects should be emphasized: (1) For the theory of auxetic sandwich plate, Lim [10] suggested that the use of classical plate theory is permitted only when the material is highly auxetic for that the auxeticity reduces shear deformation in thick plates. Ma et al. [26] believed that the accuracy of third-order shear deformation theory (TSDT) was higher than the first-order shear deformation theory (FSDT) for a moderately thick plate; (2) Internal resonance usually causes coupling of different modes, which will lead to energy transfer between different modes [27]. Due to the presence of in-plane excitation, the internal resonance can occur between two modes even though the excitation frequency is not close to any linear natural frequencies [28]; (3) A nonlinear system may have multiple solutions, the coexistence and evolution mechanism of multiple periodic solutions should be concerned, which is closely related to the second part of the well-known Hilbert's 16th problem.

In the present work, we focus our attention on a simply supported concave hexagonal composite metamaterial sandwich plate with auxetic honeycombs subjected to in-plane and transverse excitation. The method of TSDT is used to derive the two degrees of freedom nonlinear equation of motion which can be recast into a four dimensional non-autonomous system. Melnikov method is improved by combination of curvilinear coordinates and Poincaré map to detect the bifurcation and coexistence of multiple periodic vibrations as well as the parameter conditions for the plate under 1:2 internal resonance. The occurrence and disappearance of periodic orbits are analyzed in detail. Phase portraits of nonlinear vibration characteristics and waveforms of different modes for the plate in different bifurcation regions induced by transverse excitation are also obtained.

## 2 Nonlinear Equation of Motion

In this paper, a simply supported concave hexagonal composite metamaterial sandwich plate with length  $a$ , width  $b$  and thickness  $h$  is taken into account. The top and bottom face sheets of the plate are made of isotropic aluminum materials and the auxetic core layer has honeycomb structure using the same aluminum material. The thicknesses of the top, core and bottom layers are  $h_1$ ,  $h_2$  and  $h_3$ , respectively. Thus  $h = h_1 + h_2 + h_3$ . A Cartesian coordinate system  $Oxyz$  with its origin located

in the middle surface of the plate is established in which the  $x$  ( $y$ ) direction is along the length (width) of the plate, and the out-of-plane  $z$  direction points to the bottom face sheet. The mid-surface displacements of triangular plates in the  $x$ ,  $y$  and  $z$  directions are respectively represented by the symbols  $u$ ,  $v$  and  $w$ . The plate is subjected to transverse excitation of the form  $F(x, y) \cos(\Omega_1 t)$  and in-plane excitations of the form  $p_0 - p_1 \cos(\Omega_2 t)$ . The method of TSDT [29] is applied to express the displacement components

$$u(x, y, z, t) = u_0(x, y, t) + z \varphi_x(x, y, t) - \frac{4}{3h^2} z^3 \left( \varphi_x + \frac{\partial w_0}{\partial x} \right) \quad (1a)$$

$$v(x, y, z, t) = v_0(x, y, t) + z \varphi_y(x, y, t) - \frac{4}{3h^2} z^3 \left( \varphi_y + \frac{\partial w_0}{\partial y} \right) \quad (1b)$$

$$w(x, y, z, t) = w_0(x, y, t) \quad (1c)$$

where  $u_0$ ,  $v_0$  and  $w_0$  respectively represent the displacements of a point in the middle surface of the plate in  $x$ ,  $y$  and  $z$  directions.  $\varphi_x$  and  $\varphi_y$  are rotations of normals to the mid-surface with respect to the  $x$  and  $y$  axes.

The von Kármán large geometric deformation theory is taken into account to obtain the strain-displacement relations

$$\boldsymbol{\varepsilon} = \boldsymbol{\varepsilon}^0 + z \boldsymbol{\varepsilon}^1 + z^3 \boldsymbol{\varepsilon}^3, \quad \boldsymbol{\gamma} = \boldsymbol{\gamma}^0 + z^2 \boldsymbol{\gamma}^2 \quad (2)$$

where  $\boldsymbol{\varepsilon} = (\varepsilon_{xx}, \varepsilon_{yy}, \gamma_{xy})^T$ ,  $\boldsymbol{\varepsilon}^i = (\varepsilon_{xx}^i, \varepsilon_{yy}^i, \gamma_{xy}^i)^T$ ,  $\boldsymbol{\gamma} = (\gamma_{yz}, \gamma_{xz})^T$ ,  $\boldsymbol{\gamma}^j = (\gamma_{yz}^j, \gamma_{xz}^j)^T$  ( $i = 0, 1, 3; j = 0, 2$ ).  $\varepsilon_{xx}$ ,  $\varepsilon_{yy}$  are normal strains;  $\gamma_{xy}$  is the in-plane shear strain;  $\gamma_{yz}$ ,  $\gamma_{xz}$  are the transverse shear strain deformations, and

$$\begin{aligned} \varepsilon_{ii}^0 &= \frac{\partial n_i}{\partial i} + \frac{1}{2} \left( \frac{\partial w_0}{\partial i} \right)^2, & \varepsilon_{ii}^1 &= \frac{\partial \varphi_i}{\partial i}, & \varepsilon_{ii}^3 &= \frac{\partial \varphi_i}{\partial i} + \frac{\partial^2 w_0}{\partial i^2} \\ \gamma_{xy}^0 &= \frac{\partial u_0}{\partial y} + \frac{\partial v_0}{\partial x} + \frac{\partial w_0}{\partial x} \frac{\partial w_0}{\partial y}, & \gamma_{xy}^1 &= \frac{\partial \varphi_x}{\partial y} + \frac{\partial \varphi_y}{\partial x} \\ \gamma_{xy}^3 &= \frac{\partial \varphi_x}{\partial y} + \frac{\partial \varphi_y}{\partial x} + 2 \frac{\partial^2 w_0}{\partial x \partial y}, & \gamma_{iz}^0 &= \varphi_i + \frac{\partial w_0}{\partial i}, & \gamma_{iz}^2 &= -\frac{4}{h^2} \gamma_{iz}^0 \end{aligned} \quad (3)$$

where  $i = x, y$ ;  $n_i|_{i=x} = u_0$ ,  $n_i|_{i=y} = v_0$ . The expressions for stress components of the  $k$ -th ( $k = 1, 2, 3$ ) layer of the auxetic honeycomb sandwich plate are obtained by constitutive relations.

$$\begin{aligned} \boldsymbol{\sigma}_{x,y}^{(k)} &= \left( \sigma_{xx}^{(k)}, \sigma_{yy}^{(k)}, \sigma_{xy}^{(k)} \right)^T = \boldsymbol{Q}_1^{(k)} \boldsymbol{\varepsilon} \\ \boldsymbol{\sigma}_z^{(k)} &= \left( \sigma_{yz}^{(k)}, \sigma_{xz}^{(k)} \right)^T = \boldsymbol{Q}_2^{(k)} \boldsymbol{\gamma} \end{aligned} \quad (4)$$

where

$$\begin{aligned} Q_1^{(k)} &= \partial_{1,1}^{2,2} \left( \partial_{i,j}^{2,2} \left( Q_{ij}^{(k)} \right) \right) + \partial_{2,2}^{2,2} \left( Q_{66}^{(k)} \right) \\ Q_2^{(k)} &= \text{diag} \left( Q_{44}^{(k)}, Q_{55}^{(k)} \right) \end{aligned} \tag{5}$$

with

$$\begin{aligned} Q_{11}^{(k)} &= \frac{E_1^{(k)}}{1 - \nu_{12}^{(k)} \nu_{21}^{(k)}}, & Q_{22}^{(k)} &= \frac{E_2^{(k)}}{1 - \nu_{12}^{(k)} \nu_{21}^{(k)}} \\ Q_{21}^{(k)} &= Q_{12}^{(k)} = \frac{\nu_{12}^{(k)} E_1^{(k)}}{1 - \nu_{12}^{(k)} \nu_{21}^{(k)}} \\ Q_{44}^{(k)} &= G_{23}^{(k)}, & Q_{55}^{(k)} &= G_{13}^{(k)}, & Q_{66}^{(k)} &= G_{12}^{(k)} \end{aligned} \tag{6}$$

In above equations, the symbol  $\partial_{i,j}^{m,n}(\mathbf{M})$  denotes a partitioned matrix with  $m$  row blocks and  $n$  column blocks, and the  $(i, j)$ -th block is  $\mathbf{M}$ , a smaller matrix, all other blocks are zero matrices, and the symbol  $\text{diag}(\lambda_1, \dots, \lambda_m)$  denotes an  $m \times m$  diagonal matrix with the  $(i, i)$ -th element  $\lambda_i$ , i.e.  $\text{diag}(\lambda_1, \dots, \lambda_m) = \sum_{i=1}^m \partial_{i,i}^{m,m}(\lambda_i)$ , where  $i \leq m; j \leq n$  ( $i, j, m, n \in \mathbf{N}^+$ ) (see more details in Ref. [30]).  $Q_{ij}^{(k)}$  called the plane stress-reduced stiffness.  $E_1^{(k)}, E_2^{(k)}; G_{12}^{(k)}, G_{13}^{(k)}, G_{23}^{(k)}$  and  $\nu_{12}^{(k)}, \nu_{21}^{(k)}$  are the Young's modulus, shear elastic modulus, and Poisson's ratios of the skins and the core, respectively. The superscript  $k = 1, 2, 3$  represent the top outer skin, core material and bottom outer skin, respectively. The material property of the core layer are calculated by the following formulas.

$$\begin{aligned} E_1^{(2)} &= E_0 \frac{\tau^3 L_2}{(\tau^3 l_2 + l_1^2 L_4) \cos \theta}, & E_2^{(2)} &= E_0 \frac{\tau^3 l_1^2 \cos \theta}{L_2 L_5} \\ G_{12}^{(2)} &= E_0 \frac{\tau^3}{l_1 l_2 L_1 \cos \theta}, & G_{13}^{(2)} &= G_0 \frac{\tau \cos \theta}{L_2}, & G_{23}^{(2)} &= G_0 \frac{\tau(2L_2^2 + L_1 L_3)}{4l_1 L_1 L_2 \cos \theta} \\ \nu_{12}^{(2)} &= -\frac{L_6}{l_1 L_4 + \tau^2 l_2} \nu_{21}^{(2)} = -\frac{l_1 L_6 \cos^2 \theta}{L_2 L_5}, & \rho^{(2)} &= \rho_0 \frac{\tau(l_2 + 2l_1)}{2l_1 L_2 \cos \theta} \end{aligned} \tag{7}$$

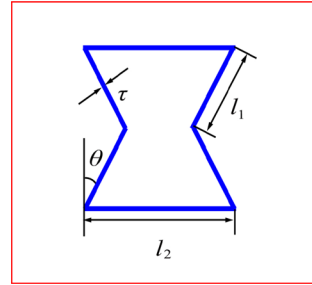
in which

$$\begin{aligned} L_1 &= l_1 + 2l_2, & L_2 &= l_2 - l_1 \sin \theta, & L_3 &= l_2 + 2l_1 \sin^2 \theta \\ L_4 &= \tau^2 \sin^2 \theta + l_1^2 \cos^2 \theta, & L_5 &= l_1^2 \sin^2 \theta + \tau^2 \cos^2 \theta, & L_6 &= (l_1^2 - \tau^2) \sin \theta \end{aligned}$$

where  $E_0, G_0$  and  $\rho_0$  are Young's modulus, shear modulus and mass density of the origin material.  $l_1$  and  $l_2$  represent the length of the inclined and horizontal cell rib of the unit cell of concave hexagonal honeycomb core.  $\tau$  is the uniform thickness of cell rib,  $\theta$  is the inclined angle. Here  $0 < \theta < \frac{\pi}{2}$  for that the unit cell possesses concave shape (auxetic) as shown in Fig. 1 [31].

The nonlinear equation of motion for the auxetic plate can be derived by Hamilton's principle, as shown in Appendix A. For the simply supported sandwich plate with NPR, the boundary conditions are expressed as follows.

**Fig. 1** Unit cell of the core structure with inclined rib length  $l_1$ , horizontal rib length  $l_2$ , inclined angle  $\theta$ , and rib thickness  $\tau$



$$\begin{aligned}
 w = 0, \varphi_y = 0, M_{xx} = N_{xy} = 0, \quad & \text{at } x = 0, a \\
 w = 0, \varphi_x = 0, M_{yy} = N_{xy} = 0, \quad & \text{at } y = 0, b \\
 \int_0^b N_{xx}|_{x=0, a} dy = \int_0^b (p_0 - p_1 \cos(\Omega_2 t)) dy & \quad (8)
 \end{aligned}$$

Consider the first two order modes of the plate, the displacements and transverse excitation can be written in the following forms.

$$u_0 = u_1 \cos \frac{3\pi x}{a} \sin \frac{\pi y}{b} + u_2 \cos \frac{\pi x}{a} \sin \frac{3\pi y}{b} \quad (9a)$$

$$v_0 = v_1 \sin \frac{3\pi x}{a} \cos \frac{\pi y}{b} + v_2 \sin \frac{\pi x}{a} \cos \frac{3\pi y}{b} \quad (9b)$$

$$w_0 = w_1 \sin \frac{3\pi x}{a} \sin \frac{\pi y}{b} + w_2 \sin \frac{\pi x}{a} \sin \frac{3\pi y}{b} \quad (9c)$$

$$F = F_1 \sin \frac{3\pi x}{a} \sin \frac{\pi y}{b} + F_2 \sin \frac{\pi x}{a} \sin \frac{3\pi y}{b} \quad (9d)$$

where  $u_i, v_i, w_i$  ( $i = 1, 2$ ) represent the amplitudes of the first two order modes, respectively;  $F_1, F_2$  represent the amplitudes of the transverse excitation corresponding to the first two order modes.

Considering the transverse motion of the auxetic honeycomb sandwich plate, a two degrees of freedom dimensionless nonlinear equation of motion for the plate in the first two order modes is obtained based on the Galerkin method.

$$\ddot{\mathbf{w}} + \boldsymbol{\omega} \mathbf{w} + \mu \boldsymbol{\alpha}_1 \dot{\mathbf{w}} + \cos(\Omega_2 t) \boldsymbol{\alpha}_2 \mathbf{w} + \mathbf{W}(\mathbf{w}) = \cos(\Omega_1 t) \mathbf{f} \quad (10)$$

where

$$\begin{aligned}
 \mathbf{w} &= (w_1, w_2)^T, \quad \boldsymbol{\omega} = \text{diag}(\omega_1^2, \omega_2^2) \\
 \boldsymbol{\alpha}_1 &= \text{diag}(\alpha_{11}, \alpha_{21}), \quad \boldsymbol{\alpha}_2 = \text{diag}(\alpha_{12}, \alpha_{22}) \\
 \mathbf{f} &= (f, f)^T, \quad \mathbf{W} = (W_1, W_2)^T \\
 W_i &= \sum_{j=0}^3 \alpha_{i(j+3)} w_i^{3-j} w_{3-i}^j \quad (i = 1, 2)
 \end{aligned}$$

$\omega_i$  are linear natural frequencies,  $\mu$  is the damping coefficient,  $f$  is the transverse excitations,  $\Omega_1$  and  $\Omega_2$  are the frequencies of transverse and in-plane excitation respectively,  $\alpha_{ij} (\neq 0)$  are non-dimensional coefficients,  $i = 1, 2; j = 1, \dots, 6$ .

Let  $x_{i1} = \omega_i w_i, x_{i2} = \dot{w}_i (i = 1, 2)$ , and introducing the scale transformations  $\alpha_{ij} \rightarrow \varepsilon \alpha_{ij}, f \rightarrow \varepsilon f (i = 1, 2; j = 1, \dots, 6)$ . The two degrees of freedom nonlinear equation can be recast into the following four dimensional non-autonomous equation.

$$\dot{\mathbf{x}} = \mathbf{A}\mathbf{x} + \varepsilon \mathbf{F}(t, \mathbf{x}) \tag{11}$$

where  $\mathbf{x} = (x_{11}, x_{12}, x_{21}, x_{22})^T \in \mathbf{R}^4, \mathbf{A} = \sum_{i,j=1}^2 \partial_{i,i}^{2,2} \left( \partial_{j,3-j}^{2,2} \left( (-1)^{j+1} \omega_i \right) \right), \mathbf{F} = (0, F_{12}, 0, F_{22})^T$  is a vector-valued function in variables of  $(x_{11}, x_{12}, x_{21}, x_{22}, t)$ , and

$$\begin{aligned}
 F_{i2} &= f \cos(\Omega_i t) - \alpha_{i1} \mu x_{i2} - \frac{\alpha_{i2}}{\omega_i} x_{i1} \cos(\Omega_2 t) \\
 &\quad - \sum_{j=0}^3 \frac{\alpha_{i(j+3)}}{\omega_i^{3-j} \omega_{3-i}^j} x_{i1}^{3-j} x_{(3-i)1}^j \quad i = 1, 2
 \end{aligned} \tag{12}$$

The following analysis should be focused on the bifurcation and coexistence of the multiple periodic vibrations and the effects of transverse excitation on the nonlinear vibration behaviors.

### 3 Multiple Periodic Vibration Analysis

In this section, Melnikov method is improved to analyze the bifurcation and coexistence of multiple periodic vibrations of system (11). When  $\varepsilon = 0$ , system (11) degenerates to two uncoupled Hamiltonian systems with Hamilton functions

$$H_i(\mathbf{x}_i) = \frac{1}{2} \omega_i (x_{i1}^2 + x_{i2}^2) \quad i = 1, 2 \tag{13}$$

where  $\mathbf{x}_i = (x_{i1}, x_{i2})^T \in \mathbf{R}^2$ . Then there exists an open interval  $\mathbf{K} \subset \mathbf{R}^2$  and  $\mathbf{h} = (h_1, h_2)^T \in \mathbf{K}$  such that each system has a family of periodic orbits in  $\mathbf{x}_i$  plane, which can be expressed as  $\Gamma_i = \left\{ \mathbf{x}_i^{h_i} \mid H_i(\mathbf{x}_i) = h_i \right\}$ , and the corresponding period is  $T_i(h_i)$ . Assuming that there exists  $\mathbf{h}_0 = (h_{10}, h_{20})^T \in \mathbf{K}$  and a pair of coprime integers  $r_i, k_i$  such that  $\frac{T_i(h_{i0})}{T} = \frac{r_i}{k_i}$ , then system (11) $_{\varepsilon=0}$  has a family of periodic orbits with period  $r_0 T$  in the invariant torus  $\Gamma_{10} \times \Gamma_{20}, r_0$  is the least common multiple of  $r_1$  and  $r_2$ .



When  $\varepsilon \neq 0$ , by defining the function  $\psi : \mathbf{R} \rightarrow \mathbf{S}$  as  $t \rightarrow t \pmod{T}$ , we can rewrite system (11) in the form of a five dimensional autonomous system, i.e. adding  $\dot{t} = 1$  in system (11). Introducing the curvilinear coordinates  $(s_1, n_1, s_2, n_2, t)$  in the sufficiently small neighborhood of the invariant torus  $\Gamma_{10} \times \Gamma_{20} \times \mathbf{S} = \mathbf{T}^3$ , where  $s_i = \int_0^t |\mathbf{J}DH_i(x_i(\tau))| d\tau$  represent the arc length of  $\Gamma_i$ ,  $\mathbf{J} = \partial_{x_i}^{2,2}((-1)^{j+1})$ ,  $i = 1, 2$ . Define a global cross section  $\Sigma = \{s_1, n_1, s_2, n_2, t \mid t = 0\}$  in the phase space  $\mathbf{R}^2 \times \mathbf{T}^3$ , and construct the  $m_0$ -th iteration of Poincaré map  $P^{m_0} : \Sigma \rightarrow \Sigma$  as  $(s_{10}, n_{10}, s_{20}, n_{20}) \rightarrow (s_1(m_0T), n_1(m_0T), s_2(m_0T), n_2(m_0T))$ , where  $s_{i0} = s_i(0)$ ,  $n_{i0} = n_i(0)$  ( $i = 1, 2$ ) are initial values. A fixed point of  $P^{m_0}$  corresponds to a periodic solution of system (11).  $(s_{10}, n_{10}, s_{20}, n_{20})$  is a fixed point if and only if

$$\begin{aligned}
 P_{i1} &= s_i(m_0T) - s_{i0} = \int_0^{m_0T} \dot{s}_i dt = 0 \\
 P_{i2} &= n_i(m_0T) - n_{i0} = \int_0^{m_0T} D_{s_i} n_i \cdot \dot{s}_i dt = 0
 \end{aligned}
 \tag{14}$$

where  $D_s = \frac{\partial}{\partial s}$ ,  $i = 1, 2$ .

Then the Melnikov function  $\mathbf{M} = (M_{11}, M_{12}, M_{21}, M_{22})^T$  will be obtained as follows [32].

$$\begin{aligned}
 M_{i1} &= \int_0^{m_0T} \frac{\omega_i^2}{2h_i} x_{i1} F_{i2} dt \\
 M_{i2} &= \int_0^{m_0T} \omega_i x_{i2} F_{i2} dt \quad i = 1, 2
 \end{aligned}
 \tag{15}$$

Thus, a fixed point of  $P^{m_0}$  is equivalent to a zero solution of the Melnikov function.

Suppose that the family of periodic orbits  $\Gamma_i (i = 1, 2)$  for system (11) $_{\varepsilon=0}$  can be expressed as

$$x_{i1} = \sqrt{\frac{2h_i}{\omega_i}} \cos(\omega_i(t + t_i)), \quad x_{i2} = \sqrt{\frac{2h_i}{\omega_i}} \sin(\omega_i(t + t_i))
 \tag{16}$$

The corresponding periods of the orbits are  $T_1(h_1) = \frac{2\pi}{\omega_1}$  and  $T_2(h_2) = \frac{2\pi}{\omega_2}$ , respectively. In this paper, we focus on the case of 1:2 internal resonance, the resonance relations satisfy

$$\omega_1 : \omega_2 : \Omega_1 : \Omega_2 = 1 : 2 : 2 : 2
 \tag{17}$$

Assuming that  $\Omega_1 = \Omega_2 = 2$ , thus  $T_1(h_1) = 2T_2(h_2) = 2\pi$ . Taking Eqs. (12) and (16) into Eq. (15), and let  $\mathbf{M}$  be zero, yields

$$M_{11} = \frac{\pi}{8} \left( 12\alpha_{13}h_1 + \alpha_{15}h_2 + 4\alpha_{12} \cos(2t_1) \right) = 0
 \tag{18a}$$

$$M_{12} = \frac{\pi}{16} \left( 16\alpha_{25}h_1 + 3\alpha_{23}h_2 - 32f \cos(2t_2) h_2^{-\frac{1}{2}} \right) = 0 \tag{18b}$$

$$M_{21} = \pi h_1 \left( 2\mu\alpha_{11} + \alpha_{12} \sin(2t_1) \right) = 0 \tag{18c}$$

$$M_{22} = 2\pi\sqrt{h_2} \left( \mu\alpha_{21}\sqrt{h_2} - f \sin(2t_2) \right) = 0 \tag{18d}$$

For convenience, we denote  $m_i = \cos(2t_i)$ ,  $n_i = \sin(2t_i)$ ,  $i = 1, 2$ .

(1) If  $f = 0$  (that is without transverse excitation), from Eqs. (18b) and (18d), we have  $h_1 = h_2 = 0$ , there is no periodic solution for system (11).

(2) If  $f \neq 0$ , we can solve

$$m_1 = -\frac{1}{4\alpha_{12}}(12\alpha_{13}h_1 + \alpha_{15}h_2), \quad n_1 = -\frac{2\mu\alpha_{11}}{\alpha_{12}} \tag{19a}$$

$$m_2 = \frac{\sqrt{h_2}}{32f}(16\alpha_{25}h_1 + 3\alpha_{23}h_2), \quad n_2 = \frac{\mu\alpha_{21}}{f}\sqrt{h_2} \tag{19b}$$

From  $m_1^2 + n_1^2 = 1$ , we can solve

$$h_1^\pm = \frac{1}{12\alpha_{13}} \left( -\alpha_{15}h_2 \pm 4\sqrt{\alpha_{12}^2 - 4\mu^2\alpha_{11}^2} \right) \stackrel{\text{def}}{=} h_\pm(h_2) \tag{20}$$

Taking Eqs. (19b) and (20) into  $m_2^2 + n_2^2 = 1$ , yields

$$g_\pm(h_2) = A^2h_2^3 \pm 2ABh_2^2 + (B^2 + C^2)h_2 - D^2 = 0 \tag{21}$$

where

$$A = 9\alpha_{13}\alpha_{23} - 4\alpha_{15}\alpha_{25}, \quad B = 16\alpha_{25}\sqrt{\alpha_{12}^2 - 4\mu^2\alpha_{11}^2}, \quad C = \mu\alpha_{21}a, \quad D = af, \quad a = 96\alpha_{13}$$

Obviously,  $CD \neq 0$ . If  $A = 0$ , then we can solve

$$h_2 = \frac{D^2}{B^2 + C^2} \tag{22}$$

There can be at most one set of positive real solution for  $(h_1, h_2)$ . Else, if  $A \neq 0$ , according to the relations between roots and coefficients of cubic equations, we have

$$h_{21} h_{22} h_{23} = \frac{D^2}{A^2}, \quad h_{21} + h_{22} + h_{23} = \mp \frac{2B}{A} \tag{23}$$

By analyzing the sign of Eq. (23), we can only get a rough estimation on the number of periodic solutions. Once the coefficients of the system (11) are given, the existence and precise number of periodic solutions can be obtained.

In this paper, we choose the coefficients as follows.

$$\begin{aligned}
 PC &= \{ \mu, \alpha_{11}, \alpha_{12}, \alpha_{13}, \alpha_{15}, \alpha_{21}, \alpha_{23}, \alpha_{25} \} \\
 &= \{ 0.2, 10, -5, 0.5, -3, 10, 0.5, -12 \}
 \end{aligned}
 \tag{24}$$

The transverse excitation  $f$  is left as a control parameter. Under this condition, we can calculate  $A = -141.75, B = -576, C = 96, D = 48f$ .

By analyzing the sign of solutions  $(h_1, h_2)$  in equations  $h_{\pm}$  (Eq. (20)) and  $g_{\pm}$  (Eq. (21)), we obtain four critical values of the parameter  $f = \pm f_1, \pm f_2$ , where

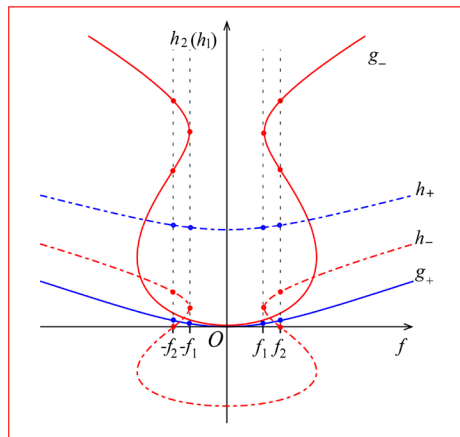
$$f_1 = \frac{32}{189} \sqrt{1890 - 231\sqrt{33}}, \quad f_2 = \frac{1}{8} \sqrt{1033}
 \tag{25}$$

The graph of the solution  $(h_1, h_2)$  changing with parameter  $f$  ( $f \neq 0$ ) is plotted in Fig. 2 which provides a visualization of the existence and number of periodic solutions.

Note that there is a one-to-one correspondence between the solutions  $h_1$  and  $h_2$ , and all the solutions of  $h_2$  for equation  $g_{\pm}$  are positive. So we can analyze the solution of  $h_1$  for equation  $h_{\pm}$  only. For equation  $h_+$ , as can be seen in Fig. 2, there is always one positive solution of  $h_1$ . For equation  $h_-$ , there is no positive solution when  $0 < |f| < f_1$ , one positive solution when  $|f| = f_1$ , two positive solutions when  $f_1 < |f| < f_2$ , one positive and one zero solution when  $|f| = f_2$ , and one positive solution when  $|f| > f_2$ .

For convenience, we classify the periodic solutions obtained from  $h_+$  and  $g_+$  as family  $\Gamma^+$ , and classify the periodic solutions obtained from  $h_-$  and  $g_-$  as family  $\Gamma^-$ . Thus, there will be always one periodic solution in family  $\Gamma^+$ . For family  $\Gamma^-$ , there is no periodic solution when  $0 < |f| < f_1$ , one periodic solution when  $|f| = f_1$ , two periodic solutions when  $f_1 < |f| \leq f_2$  and one periodic solution when  $|f| > f_2$ . In summary, there can be at most three periodic solutions for the system in a certain bifurcation region.

**Fig. 2** Variation of the solutions  $h_1$  and  $h_2$  with  $f$  under condition  $PC: \pm f_1, \pm f_2$  are critical values



## 4 Numerical Simulations

There will be interactions between the first two order modes of the system, and the energy will be transferred between them. In this section, the patterns of multiple periodic vibrations and waveforms of the first two order modes are presented graphically to reveal the vibration law and energy transfer styles for the system as the parameter varies from one region to another.

(1)  $f = 0$

Recall that, when  $f = 0$ , i.e. without transverse excitation, there is no periodic orbit under condition  $PC$ . The phase portraits are shown in Fig. 3, where Fig. 3a, b represent the two and three dimensional projections, respectively. As shown in these figures, the solution curves are densely distributed, and no closed orbit can be found in the portraits.

(2)  $0 < |f| < f_1$

There is one periodic orbit when  $0 < |f| < f_1$  under condition  $PC$ , denote as  $\Gamma_1$  ( $\in \Gamma^+$ ). The phase portraits are shown in Fig. 4, where Fig. 4a, b represent the two dimensional projections, Fig. 4c, d represent the three dimensional projections. One closed orbit can be found in each portrait, and the spiral form of the orbit is clearly visible. Figure 5 shows the waveforms of  $w_1$  mode and  $w_2$  mode of the periodic orbit  $\Gamma_1$  when  $0 < |f| < f_1$  under condition  $PC$ . In the first half of the period,  $w_1$  and  $w_2$  increase simultaneously in a certain time range, whereafter  $w_1$  keeps increasing and  $w_2$  will decrease and then increase again.  $w_2$  nearly equals to zero when  $w_1$  reaches its peak. After the peak, in the second half of the period,  $w_1$  decreases gradually,  $w_2$  changes in the same way as before and nearly equals to zero when  $w_1$  reaches its valley.

(3)  $|f| = f_1$

When  $|f|$  increases gradually and reaches  $|f| = f_1$ , bifurcation occurs and a new periodic orbit  $\Gamma_2$  ( $\in \Gamma^-$ ) generated. Then there exist two periodic orbits when  $|f| = f_1$  under condition  $PC$ . The phase portraits of periodic vibrations are shown in Fig. 6, where Fig. 6a, b represent the two dimensional projections, Fig. 6c, d represent the three dimensional projections. Figure 7 shows the waveforms of

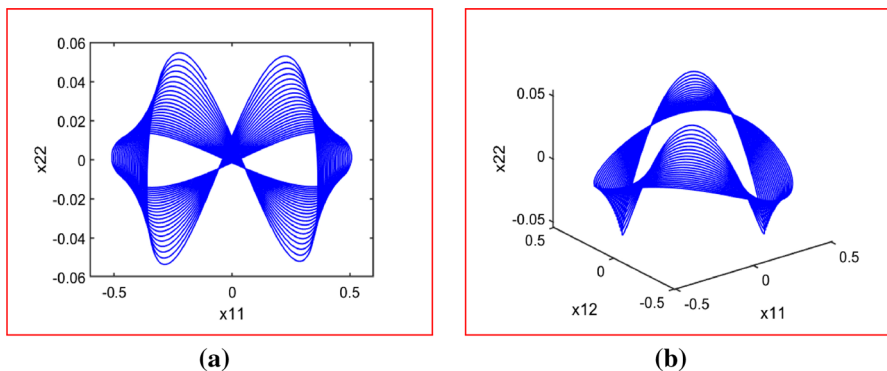
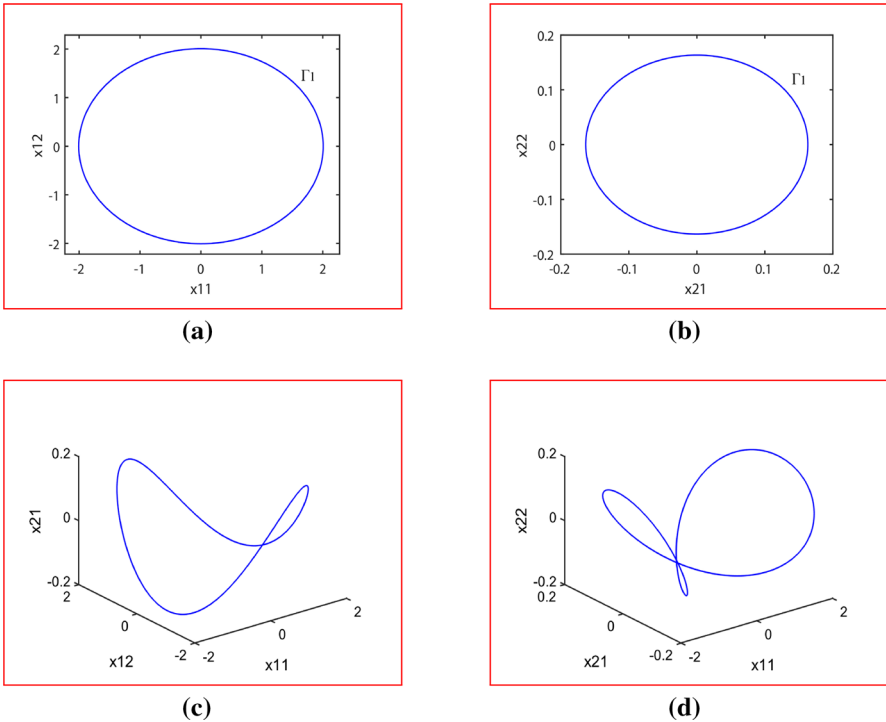
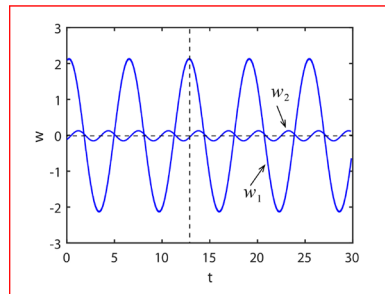


Fig. 3 Phase portraits of  $f = 0$ : (a)  $(x_{11}, x_{22})$ -plane; (b)  $(x_{11}, x_{12}, x_{22})$ -space



**Fig. 4** Phase portraits of one periodic orbit when  $0 < |f| < f_1$ : **(a)**  $(x_{11}, x_{12})$ -plane; **(b)**  $(x_{21}, x_{22})$ -plane; **(c)**  $(x_{11}, x_{12}, x_{21})$ -space; **(d)**  $(x_{11}, x_{21}, x_{22})$ -space

**Fig. 5** Waveforms of  $w_1$  and  $w_2$  modes of  $\Gamma_1$  when  $0 < |f| < f_1$



$w_1$  mode and  $w_2$  mode of periodic vibration  $\Gamma_1$  (Fig. 7a) and  $\Gamma_2$  (Fig. 7b). Compared with Fig. 5, the energy transfer style between  $w_1$  and  $w_2$  mode of  $\Gamma_1$  ( $\in \Gamma^+$ ) when  $|f| = f_1$  is similar to that of  $\Gamma_1$  when  $0 < |f| < f_1$ . However, the energy transfer style between  $w_1$  and  $w_2$  mode of  $\Gamma_2$  ( $\in \Gamma^-$ ) is quite different from that of  $\Gamma_1$  ( $\in \Gamma^+$ ). As shown in Fig. 7b, when  $w_2$  reaches its peak,  $w_1$  will reach the peak or valley at the same time; when  $w_2$  reaches its valley,  $w_1$  nearly equals to zero.

(4)  $f_1 < |f| < f_2$

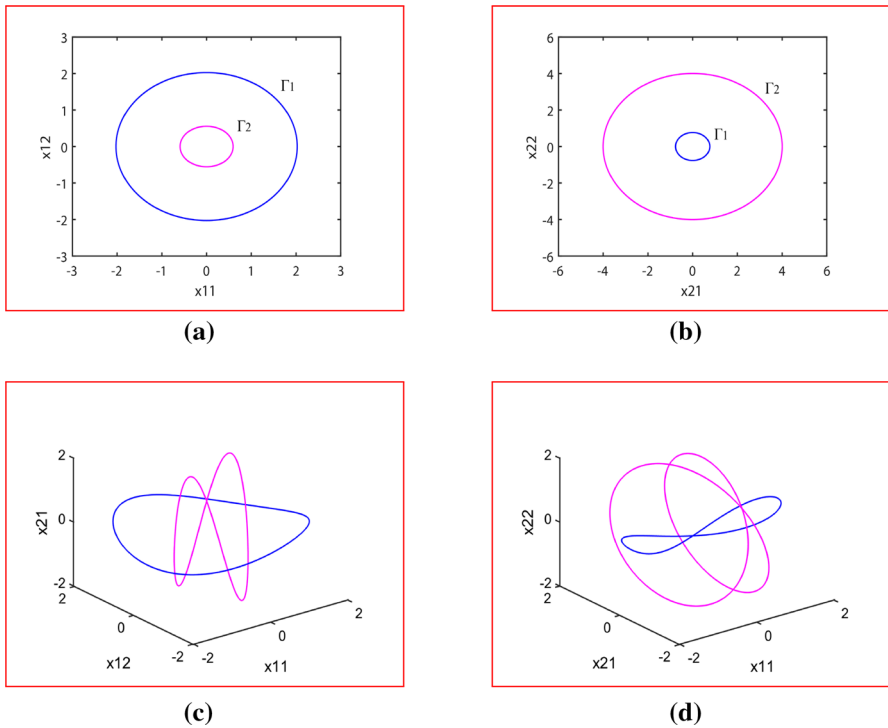


**Fig. 6** Phase portraits of periodic orbits when  $|f| = f_1$ : **(a)**  $(x_{11}, x_{12})$ -plane; **(b)**  $(x_{21}, x_{22})$ -plane; **(c)**  $(x_{11}, x_{12}, x_{21})$ -space; **(d)**  $(x_{11}, x_{21}, x_{22})$ -space

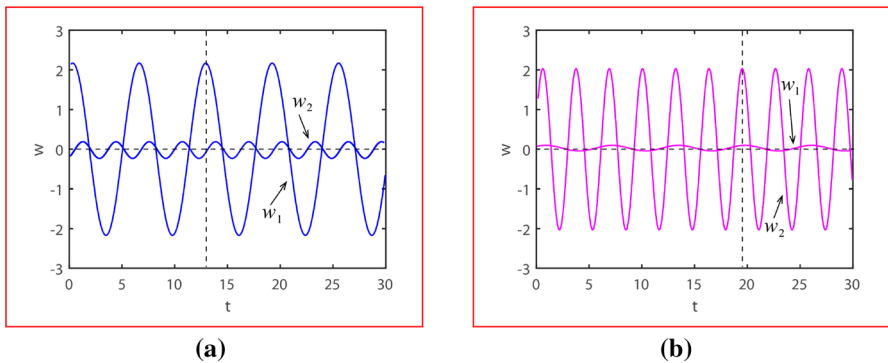


**Fig. 7** Waveforms of  $w_1$  and  $w_2$  modes of **(a)**  $\Gamma_1$  and **(b)**  $\Gamma_2$  when  $|f| = f_1$

When  $|f|$  passes the critical value  $f_1$ , the periodic orbit  $\Gamma_2$  will split into two periodic orbits immediately, denote as  $\Gamma_{21}$  and  $\Gamma_{22}$ . Thus, there are total three periodic orbits when  $f_1 < |f| < f_2$  under condition *PC*. The phase portraits are shown in Fig. 8, where Fig. 8a, b represent the two dimensional projections, Fig. 8c, d

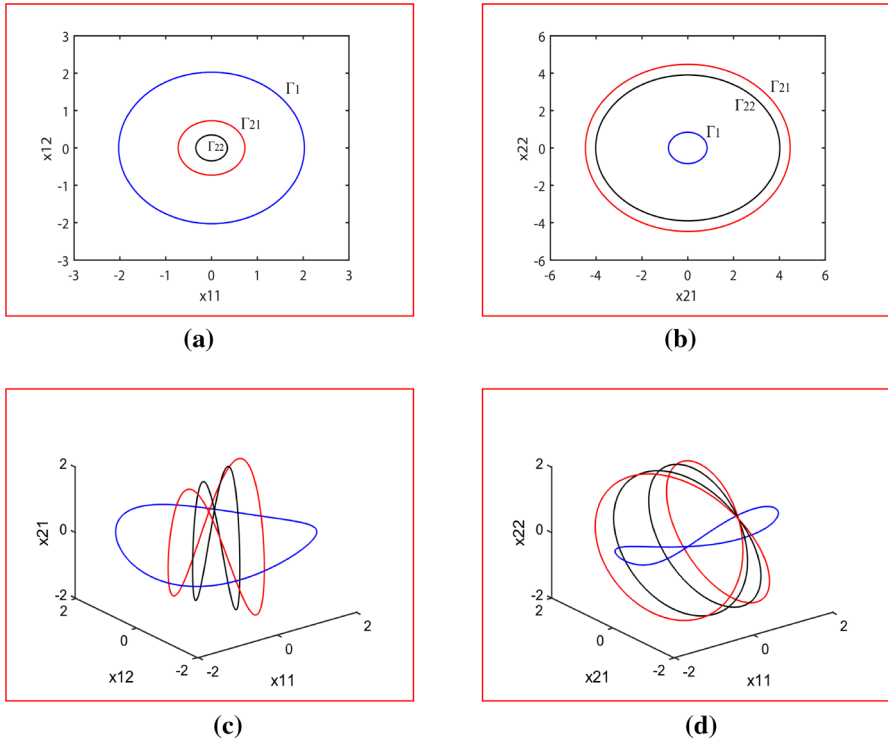


**Fig. 8** Phase portraits of periodic orbits when  $f_1 < |f| < f_2$ : **(a)**  $(x_{11}, x_{12})$ -plane; **(b)**  $(x_{21}, x_{22})$ -plane; **(c)**  $(x_{11}, x_{12}, x_{21})$ -space; **(d)**  $(x_{11}, x_{21}, x_{22})$ -space

represent the three dimensional projections. With the increase of transverse excitation, the amplitude of  $\Gamma_{21}$  increases whereas the amplitude of  $\Gamma_{22}$  decreases gradually. Figure 9 shows the waveforms of  $w_1$  mode and  $w_2$  mode of periodic vibration  $\Gamma_1$  (Fig. 9a),  $\Gamma_{21}$  (Fig. 9b) and  $\Gamma_{22}$  (Fig. 9c). Compared with Fig. 7, the energy transfer style between  $w_1$  and  $w_2$  mode of  $\Gamma_1 (\in \Gamma^+)$  when  $f_1 < |f| < f_2$  is similar to that of  $\Gamma_1$  when  $|f| = f_1$ . The energy transfer styles between  $w_1$  and  $w_2$  mode of  $\Gamma_{21}$  and  $\Gamma_{22}$  ( $\in \Gamma^-$ ) are similar to that of  $\Gamma_2 (\in \Gamma^-)$  when  $|f| = f_1$ , but quite different from that of  $\Gamma_1 (\in \Gamma^+)$ .

$$(5) |f| = f_2$$

When  $|f|$  increases continuously and reaches  $|f| = f_2$ , the Hamiltonian  $\mathbf{h} = (h_1, h_2)$  of  $\Gamma_{22}$  satisfies  $h_1 = 0, h_2 > 0$ . Thus, there are still three periodic orbits for the system when  $|f| = f_2$  under condition *PC*. The phase portraits are shown in Fig. 10, where Fig. 10a, b represent the two dimensional projections, Fig. 10c, d represent the three dimensional projections. As shown in Fig. 10a, the projection of orbit  $\Gamma_{22}$  on  $(x_{11}, x_{12})$ -plane degenerates to a point because  $h_1 = 0$ . Figure 11 shows the waveforms of  $w_1$  mode and  $w_2$  mode of periodic vibration  $\Gamma_1$  (Fig. 11a),  $\Gamma_{21}$  (Fig. 11b) and  $\Gamma_{22}$  (Fig. 11c). Compared with Fig. 9, the energy transfer style between  $w_1$  and  $w_2$  mode of  $\Gamma_1 (\in \Gamma^+)$  when  $|f| = f_2$  is similar to that

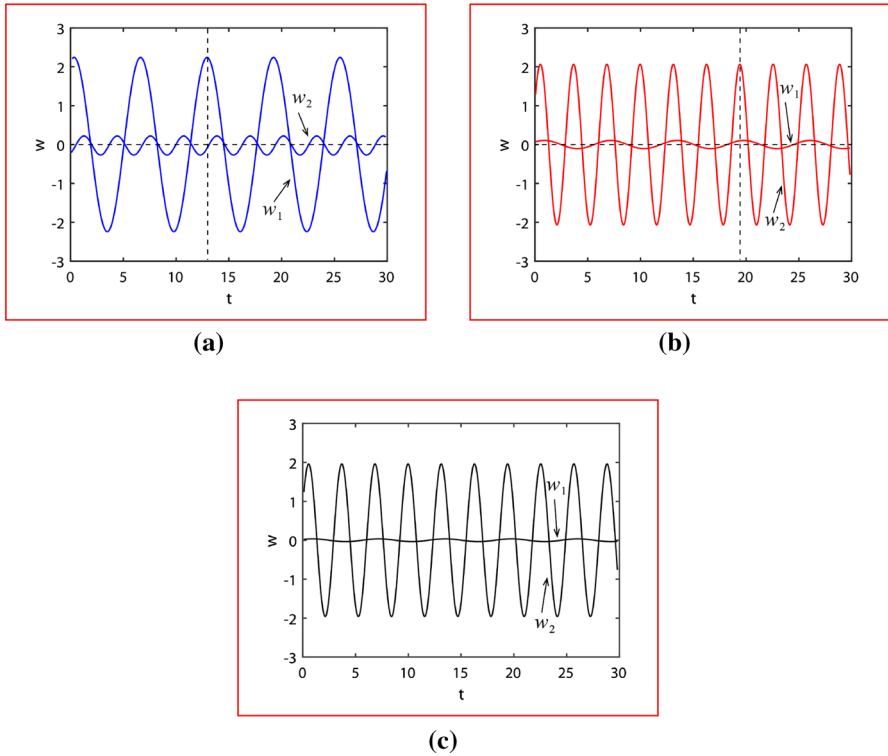


**Fig. 9** Waveforms of  $w_1$  and  $w_2$  modes of (a)  $\Gamma_1$ , (b)  $\Gamma_{21}$  and (c)  $\Gamma_{22}$  when  $f_1 < |f| < f_2$

of  $\Gamma_1$  when  $f_1 < |f| < f_2$ . The energy transfer styles between  $w_1$  and  $w_2$  mode of  $\Gamma_{21}$  and  $\Gamma_{22}$  ( $\in \Gamma^-$ ) are similar to that of  $\Gamma_{21}$  and  $\Gamma_{22}$  ( $\in \Gamma^-$ ) when  $f_1 < |f| < f_2$ , but different from that of  $\Gamma_1$  ( $\in \Gamma^+$ ).

(6)  $|f| > f_2$

When  $|f|$  passes the critical value  $f_2$ , the periodic orbit  $\Gamma_{22}$  vanishes immediately. So, there are only two periodic orbits remain ( $\Gamma_1$  and  $\Gamma_{21}$ ) when  $|f| > f_2$  under condition *PC*. The phase portraits are shown in Fig. 12, where Fig. 12a, b represent the two dimensional projections, Fig. 12c, d represent the three dimensional projections. Figure 13 shows the waveforms of  $w_1$  mode and  $w_2$  mode of periodic vibration  $\Gamma_1$  (Fig. 13a) and  $\Gamma_{21}$  (Fig. 13b). The energy transfer style between  $w_1$  and  $w_2$  mode of  $\Gamma_1$  ( $\in \Gamma^+$ ) when  $|f| > f_2$  is similar to that of  $\Gamma_1$  when  $|f| = f_2$ . The energy transfer style between  $w_1$  and  $w_2$  mode of  $\Gamma_{21}$  ( $\in \Gamma^-$ ) when  $|f| > f_2$  is similar to that of  $\Gamma_{21}$  when  $|f| = f_2$ , but quite different to that of  $\Gamma_1$ .

From the above analysis, there exists one periodic orbit ( $\Gamma_1$ ) when  $0 < |f| < f_1$  for the system under 1:2 internal resonance. With the increase of excitation  $|f|$ , the amplitude of  $\Gamma_1$  increases gradually. Another periodic orbit ( $\Gamma_2$ ) occurs at the critical parameter value  $|f| = f_1$ , and then immediately splits into two periodic orbits ( $\Gamma_{21}$  and  $\Gamma_{22}$ ) once the excitation  $|f|$  passes  $f_1$ . The amplitude of  $\Gamma_{21}$  increases



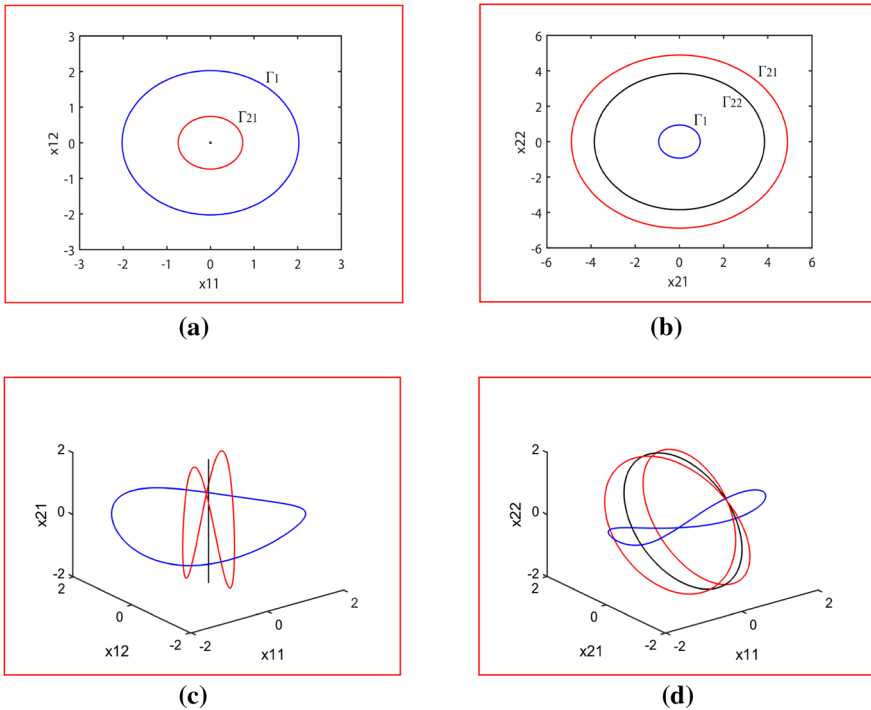


**Fig. 10** Phase portraits of periodic orbits when  $|f| = f_2$ : (a)  $(x_{11}, x_{12})$ -plane; (b)  $(x_{21}, x_{22})$ -plane; (c)  $(x_{11}, x_{12}, x_{21})$ -space; (d)  $(x_{11}, x_{21}, x_{22})$ -space

whereas the amplitude of  $\Gamma_{22}$  decreases as the parameter value  $|f|$  continues to increase, and the periodic orbit  $\Gamma_{22}$  will disappear immediately when  $|f|$  passes  $f_2$ . From then on, there remain only two periodic orbits  $\Gamma_1$  and  $\Gamma_{21}$ , and their amplitudes will increase gradually with the increase of excitation  $|f|$ . The detailed evolution law of periodic orbits (including number and amplitude) changing with parameter  $f$  can be seen intuitively in the phase-parameter space (see Fig. 14). The number of periodic orbits changes as:  $2 \rightarrow 3 \rightarrow 2 \rightarrow 1 \rightarrow 0 \rightarrow 1 \rightarrow 2 \rightarrow 3 \rightarrow 2$ . They are classified into two families:  $\Gamma^+$  and  $\Gamma^-$ . The energy transfer style between  $w_1$  mode and  $w_2$  mode is similar for the orbits in the same family but quite different for the orbits in different families.

## 5 Conclusions

Sandwich plates in auxetic honeycombs with special properties can meet the need of modern science and technology development and have been widely used in aerospace, defense and other industries. When they are used as the horizontal retaining or vertical bearing structures, the plates have to carry complex loads in the service process which would lead to performance degradation or produce

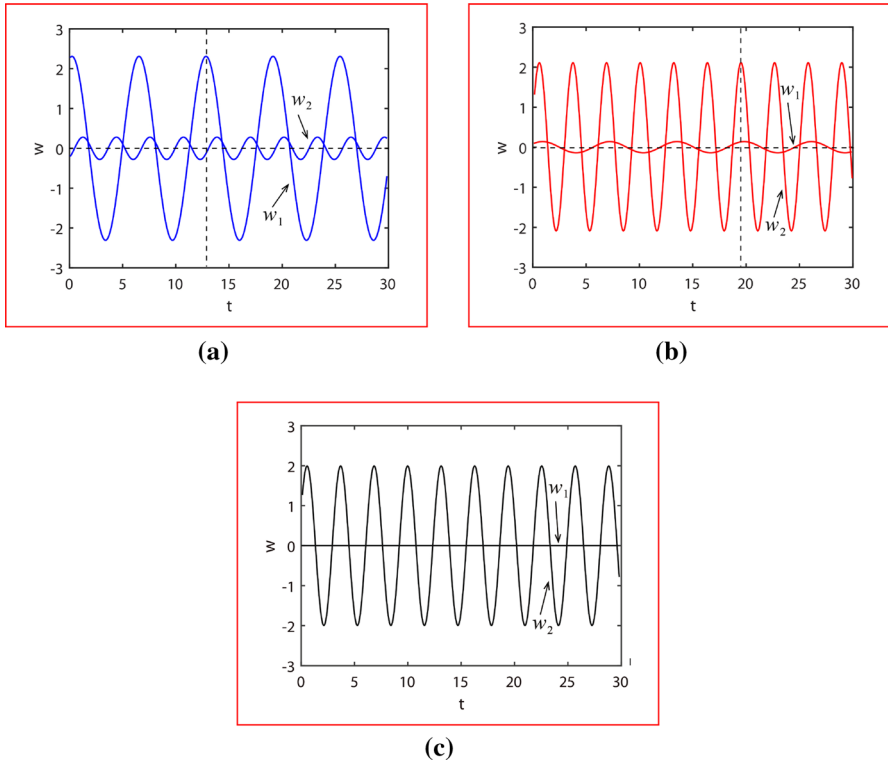
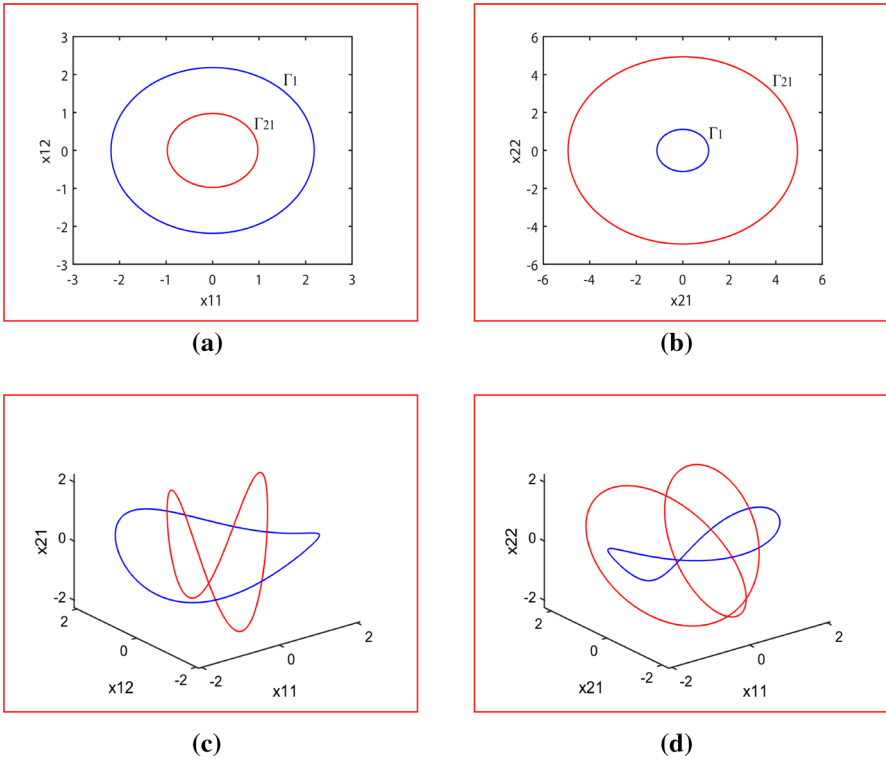


Fig. 11 Waveforms of  $w_1$  and  $w_2$  modes of (a)  $\Gamma_1$ , (b)  $\Gamma_{21}$  and (c)  $\Gamma_{22}$  when  $|f| = f_2$

structural damages. A major concern in the design and construction stages is to predict the force and vibration behaviors.

In this paper, multiple periodic vibrations of auxetic honeycomb sandwich plates subjected to in-plane and transverse excitation are investigated. The two degrees of freedom nonlinear equation of motion for the plate is derived based on TSDT and von Kármán type nonlinear geometric assumptions. The 1:2 internal resonance is taken into account to analyze the bifurcation and coexistence of multiple periodic orbits with the extended Melnikov method. Phase portraits of geometric structures and waveforms of multiple periodic vibrations in different bifurcation regions induced by transverse excitation are obtained with numerical method. The changes of number and amplitude of the multiple periodic orbits are intuitive described in the phase-parameter bifurcation portrait. Through this investigation, some remarks can be listed as follows:

- Without transverse excitation, there will be no periodic vibrations. Even quite small transverse excitation can cause small amplitude periodic vibration.



**Fig. 12** Phase portraits of periodic orbits when  $|f| > f_2$ : (a)  $(x_{11}, x_{12})$ -plane; (b)  $(x_{21}, x_{22})$ -plane; (c)  $(x_{11}, x_{12}, x_{21})$ -space; (d)  $(x_{11}, x_{21}, x_{22})$ -space

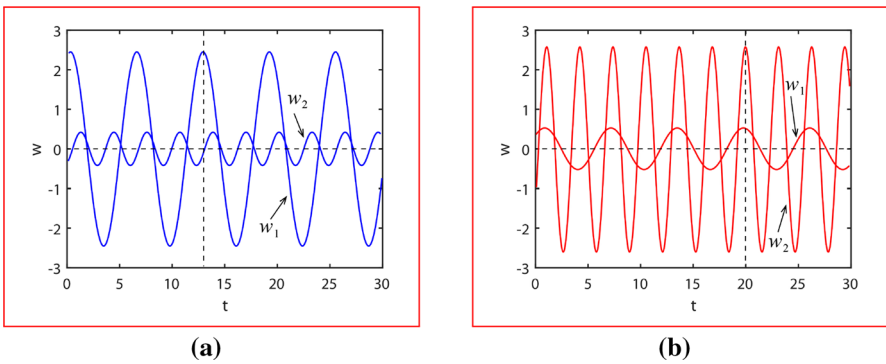


**Fig. 13** Waveforms of  $w_1$  and  $w_2$  modes of (a)  $\Gamma_1$  and (b)  $\Gamma_{21}$  when  $|f| > f_2$

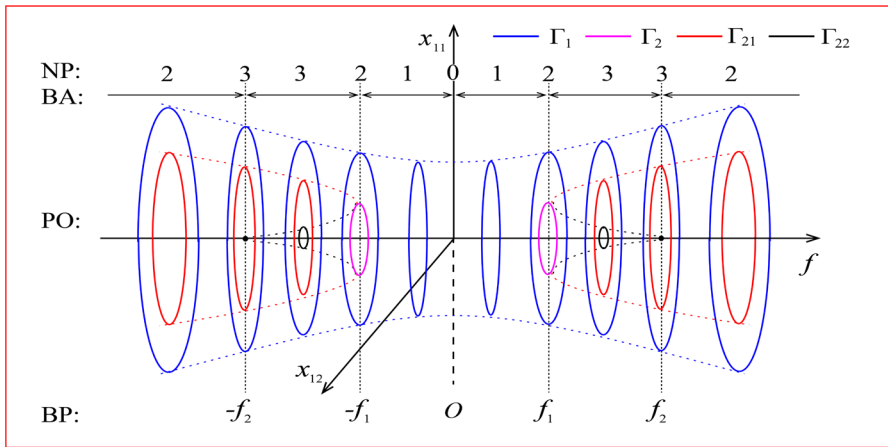


**Fig. 14** Bifurcation of multiple periodic orbits in the  $(f, x_{11}, x_{12})$  phase-parameter space under condition *PC*: NP represents the number of the periodic orbit, BA represents the bifurcation areas, PO represents the periodic orbits and BP represents the bifurcation parameter values

The amplitudes of some certain vibrations will increase gradually with the increase of excitation.

- Effects of transverse excitation on nonlinear vibration behaviors are discussed in detail. Five bifurcation values of the parameter  $f$  can be found under condition *PC* for the system:  $f = 0, \pm f_1, \pm f_2$ .
- Numerical results show that the system displays different vibration properties as the parameter varies from one bifurcation region to another, and there can be at most three periodic orbits coexisting under certain conditions.
- The periodic vibrations are classified into two families. By comparing the waveform portraits with each other, the energy transfer style between  $w_1$  mode and  $w_2$  mode is similar for the orbits in the same family but quite different for the orbits in different families.
- The current method can trace the source of periodic solutions, which provides the possibility for the classification study on generation mechanism of system complexity and energy transfers.

### Appendix A

The nonlinear equation of motion for the auxetic plate derived by Hamilton’s principle is as follows.

$$\frac{\partial N_{xx}}{\partial x} + \frac{\partial N_{xy}}{\partial y} = I_0 \ddot{u}_0 + \left( I_1 - \frac{4}{3h^2} I_3 \right) \ddot{\varphi}_x - \frac{4}{3h^2} I_3 \frac{\partial \ddot{w}_0}{\partial x} \tag{A1a}$$

$$\frac{\partial N_{yy}}{\partial y} + \frac{\partial N_{xy}}{\partial x} = I_0 \ddot{w}_0 + \left( I_1 - \frac{4}{3h^2} I_3 \right) \ddot{\phi}_y - \frac{4}{3h^2} I_3 \frac{\partial \dot{w}_0}{\partial y} \tag{A1b}$$

$$\begin{aligned} & \left( \frac{\partial N_{yy}}{\partial y} \frac{\partial w_0}{\partial y} + N_{yy} \frac{\partial^2 w_0}{\partial y^2} \right) + \left( \frac{\partial N_{xy}}{\partial x} \frac{\partial w_0}{\partial y} + 2N_{xy} \frac{\partial^2 w_0}{\partial x \partial y} + \frac{\partial N_{xy}}{\partial y} \frac{\partial w_0}{\partial x} \right) \\ & + \left( \frac{\partial N_{xx}}{\partial x} \frac{\partial w_0}{\partial x} + N_{xx} \frac{\partial^2 w_0}{\partial x^2} \right) + \frac{4}{3h^2} \left( \frac{\partial^2 P_{xx}}{\partial x^2} + 2 \frac{\partial^2 P_{xy}}{\partial x \partial y} + \frac{\partial^2 P_{yy}}{\partial y^2} \right) \\ & + \left( \frac{\partial Q_x}{\partial x} - \frac{4}{h^2} \frac{\partial R_x}{\partial x} \right) + \left( \frac{\partial Q_y}{\partial y} - \frac{4}{h^2} \frac{\partial R_y}{\partial y} \right) + F - \mu \dot{w}_0 \\ & = I_0 \ddot{w}_0 + \frac{4}{3h^2} I_3 \left( \frac{\partial \ddot{u}_0}{\partial x} + \frac{\partial \ddot{v}_0}{\partial y} \right) - \frac{16}{9h^4} I_6 \left( \frac{\partial^2 \dot{w}_0}{\partial x^2} + \frac{\partial^2 \dot{w}_0}{\partial y^2} \right) \\ & + \frac{4}{3h^2} \left( I_4 - \frac{4}{3h^2} I_6 \right) \left( \frac{\partial \dot{\phi}_x}{\partial x} + \frac{\partial \dot{\phi}_y}{\partial y} \right) \end{aligned} \tag{A1c}$$

$$\begin{aligned} & \frac{\partial M_{xx}}{\partial x} + \frac{\partial M_{xy}}{\partial y} - \frac{4}{3h^2} \left( \frac{\partial P_{xx}}{\partial x} + \frac{\partial P_{xy}}{\partial y} \right) - \left( Q_x - \frac{4}{h^2} R_x \right) \\ & = \left( I_1 - \frac{4}{3h^2} I_3 \right) \ddot{u}_0 + \left( I_2 - \frac{8}{3h^2} I_4 + \frac{16}{9h^4} I_6 \right) \dot{\phi}_x \\ & - \frac{4}{3h^2} \left( I_4 - \frac{4}{3h^2} I_6 \right) \frac{\partial \dot{w}_0}{\partial x} \end{aligned} \tag{A1d}$$

$$\begin{aligned} & \frac{\partial M_{yy}}{\partial y} + \frac{\partial M_{xy}}{\partial x} - \frac{4}{3h^2} \left( \frac{\partial P_{yy}}{\partial y} + \frac{\partial P_{xy}}{\partial x} \right) - \left( Q_y - \frac{4}{h^2} R_y \right) \\ & = \left( I_1 - \frac{4}{3h^2} I_3 \right) \ddot{v}_0 + \left( I_2 - \frac{8}{3h^2} I_4 + \frac{16}{9h^4} I_6 \right) \dot{\phi}_y \\ & - \frac{4}{3h^2} \left( I_4 - \frac{4}{3h^2} I_6 \right) \frac{\partial \dot{w}_0}{\partial y} \end{aligned} \tag{A1e}$$

where  $\mu$  is damping coefficient, and

$$\begin{aligned} I_i &= \sum_{k=1}^3 \int_{z_k}^{z_{k+1}} \rho^{(k)} z^i dz, \quad i = 0, 1, 2, \dots, 6 \\ z_1 &= -h_1 - \frac{h_2}{2}, \quad z_2 = -\frac{h_2}{2}, \quad z_3 = \frac{h_2}{2}, \quad z_4 = \frac{h_2}{2} + h_3 \end{aligned} \tag{A2}$$

The internal-strain relations are expressed as

$$\begin{aligned} N_{x,y} &= A_1 \epsilon^0, \quad Q_{x,y} = A_2 \gamma^0, \quad M_{x,y} = D_1 \epsilon^1 + F_1 \epsilon^2 \\ P_{x,y} &= F_1 \epsilon^1 + H_1 \epsilon^2, \quad R_{x,y} = D_2 \gamma^0 + F_2 \gamma^2 \end{aligned} \tag{A3}$$

in which

$$\begin{aligned} X_{x,y} &= (X_{xx}, X_{yy}, X_{xy})^T, & Y_{x,y} &= (Y_y, Y_x)^T \\ Z_1 &= \partial_{1,1}^{2,2}(\partial_{i,j}^{2,2}(Z_{ij})) + \partial_{2,2}^{2,2}(Z_{66}), & Z_2 &= \partial_{1,1}^{2,2}(Z_{44}) + \partial_{2,2}^{2,2}(Z_{55}) \\ X &= N, M, P; & Y &= Q, R; & Z &= A, D, F \end{aligned}$$

The stiffness coefficients are defined as

$$(A_{ij}, B_{ij}, D_{ij}, E_{ij}, F_{ij}, H_{ij}) = \sum_{k=1}^3 \int_{z_k}^{z_{k+1}} Q_{ij}^{(k)}(1, z, z^2, z^3, z^4, z^6) dz \quad (A4)$$

**Open Access** This article is distributed under the terms of the Creative Commons Attribution 4.0 International License (<http://creativecommons.org/licenses/by/4.0/>), which permits unrestricted use, distribution, and reproduction in any medium, provided you give appropriate credit to the original author(s) and the source, provide a link to the Creative Commons license, and indicate if changes were made.

**Author contributions** All authors typed, read, reviewed, and approved the final manuscript.

**Funding** The research project is supported by National Natural Science Foundation of China (11772007, 11290152) and also supported by Beijing Natural Science Foundation (1172002, Z180005), and the High-level Foreign Experts Funding Program of Beijing (J202134).

**Availability of data and materials** No data were used for this work.

## Declarations

**Conflict of interest** The authors declare no conflict of interest.

**Open Access** This article is licensed under a Creative Commons Attribution 4.0 International License, which permits use, sharing, adaptation, distribution and reproduction in any medium or format, as long as you give appropriate credit to the original author(s) and the source, provide a link to the Creative Commons licence, and indicate if changes were made. The images or other third party material in this article are included in the article’s Creative Commons licence, unless indicated otherwise in a credit line to the material. If material is not included in the article’s Creative Commons licence and your intended use is not permitted by statutory regulation or exceeds the permitted use, you will need to obtain permission directly from the copyright holder. To view a copy of this licence, visit <http://creativecommons.org/licenses/by/4.0/>.

## References

1. Birman, V., Kardomateas, G.A.: Review of current trends in research and applications of sandwich structures. *Compos. Part B-Eng.* **142**, 221–240 (2018)
2. Evans, K.E.: Auxetic polymers: a new range of materials. *Endeavour* **15**, 170–174 (1991)
3. Gibson, L.J., Ashby, M.F., Schajer, G.S., Roberson, C.I.: The mechanics of two-dimensional cellular materials. *Proc. R. Soc. Lond. A* **382**, 25–42 (1982)
4. Lakes, R.: Response: negative Poisson’s ratio materials. *Science* **238**, 551 (1987)
5. Milton, G.W.: Composite materials with Poisson’s ratios close to -1. *J. Mech. Phys. Solids* **40**, 1105–1137 (1992)
6. Grima, J.N., Evans, K.E.: Auxetic behavior from rotating triangles. *J. Mater. Sci.* **41**, 3193–3196 (2006)

7. Prawoto, Y.: Seeing auxetic materials from the mechanics point of view: a structural review on the negative Poisson's ratio. *Comput. Mater. Sci.* **58**, 140–153 (2012)
8. Greaves, G.N., Greer, A.L., Lakes, R.S., Rouxel, T.: Poisson's ratio and modern materials. *Nat. Mater.* **10**, 823–837 (2011)
9. Lim, T.C.: Circular auxetic plates. *J. Mech.* **29**, 121–133 (2012)
10. Lim, T.C.: Shear deformation in thick auxetic plates. *Smart Mater. Struct.* **22**, 084001 (2013)
11. Dong, Z.C., Li, Y., Zhao, T., Wu, W.W., Xiao, D.B., Liang, J.: Experimental and numerical studies on the compressive mechanical properties of the metallic auxetic reentrant honeycomb. *Mater. Design* **182**, 108036 (2019)
12. Lakes, R.S., Elms, K.: Indentability of conventional and negative Poisson's ratio foams. *J. Compos. Mater.* **27**, 1193–1202 (1993)
13. Alderson, K.L., Fitzgerald, A., Evans, K.E.: The strain dependent indentation resilience of auxetic microporous polyethylene. *J. Mater. Sci.* **35**, 4039–4047 (2000)
14. Choi, J.B., Lakes, R.S.: Fracture toughness of re-entrant foam materials with a negative Poisson's ratio: experiment and analysis. *Int. J. Fract.* **80**, 73–83 (1996)
15. Mueller, J., Raney, J.R., Shea, K., Lewis, J.A.: Architected lattices with high stiffness and toughness via multicore-shell 3D printing. *Adv. Mater.* **30**, 1705001 (2018)
16. Mohsenizadeh, S., Alipour, R., Rad, M.S., Nejad, A.F., Ahmad, Z.: Crashworthiness assessment of auxetic foam-filled tube under quasi-static axial loading. *Mater. Des.* **88**, 258–268 (2015)
17. Lu, G., Yu, T.X.: Energy absorption of structures and materials. Woodhead Publishing Ltd., Cambridge (2003)
18. Qiao, J.X., Chen, C.Q.: Impact resistance of uniform and functionally graded auxetic double arrow head honeycombs. *Int. J. Impact Eng.* **83**, 47–58 (2015)
19. Bonatti, C., Mohr, D.: Smooth-shell metamaterials of cubic symmetry: anisotropic elasticity, yield strength and specific energy absorption. *Acta. Mater.* **164**, 301–321 (2019)
20. Yang, S., Qi, C., Wang, D., Gao, R.J., Hu, H.T., Shu, J.: A comparative study of ballistic resistance of sandwich panels with aluminum foam and auxetic honeycomb cores. *Adv. Mech. Eng.* **5**, 589216 (2013)
21. Imbalzano, G., Linforth, S., Ngo, T.D., Lee, P.V.S., Tran, P.: Blast resistance of auxetic and honeycomb sandwich panels: comparisons and parametric designs. *Compos. Struct.* **183**, 242–261 (2018)
22. Zhang, J.H., Zhu, X.F., Yang, X.D., Zhang, W.: Transient nonlinear responses of an auxetic honeycomb sandwich plate under impact loads. *Int. J. Impact Eng.* **134**, 103383 (2019)
23. Streck, T., Jopek, H., Nienartowicz, M.: Dynamic response of sandwich panels with auxetic cores. *Phys. Status Solidi B* **252**, 1540–1550 (2015)
24. Zhu, X.F., Zhang, J.H., Zhang, W., Chen, J.: Vibration frequencies and energies of an auxetic honeycomb sandwich plate. *Mech. Adv. Mater. Struct.* **26**, 1951–1957 (2019)
25. Quyen, N.V., Thanh, N.V., Quan, T.Q., Duc, N.D.: Nonlinear forced vibration of sandwich cylindrical panel with negative Poisson's ratio auxetic honeycombs core and CNTRC face sheets. *Thin-Walled Struct.* **162**, 107571 (2021)
26. Ma, Y.L., Gao, Y.H., Yang, W.L., He, D.: Free vibration of a micro-scale composite laminated Reddy plate using a finite element method based on the new modified couple stress theory. *Results Phys.* **16**, 102903 (2020)
27. Nayfeh, A.H., Mook, D.T.: Nonlinear oscillations. Wiley-Interscience, New York (1979)
28. Sun, M., Quan, T.T., Wang, D.M.: Nonlinear oscillations of rectangular plate with 1:3 internal resonance between different modes. *Results Phys.* **11**, 495–500 (2018)
29. Reddy, J.N.: Mechanics of laminated composite plates and shells: theory and analysis, 2nd edn. CRC Press, Boca Raton (2003)
30. Li, J., Zhang, L.N., Wang, D.: Unique normal form of a class of 3 dimensional vector fields with symmetries. *J. Differ. Equ.* **257**, 2341–2359 (2014)
31. Lim, T.C.: Auxetic materials and structures. Springer, Singapore (2015)
32. Quan, T.T., Li, J., Zhang, W., Sun, M.: Bifurcation and number of subharmonic solutions of a 2n-dimensional non-autonomous system and its application. *Nonlinear Dyn.* **98**, 301–315 (2019)